Proceedings of International Conference on Heat Exchanger Fouling and Cleaning - 2013 (Peer-reviewed)
June 09 - 14, 2013, Budapest, Hungary
Editors: M.R. Malayeri, H. Müller-Steinhagen and A.P. Watkinson
Published online
www.heatexchanger-fouling.com

MODELLING TURBULENCE AND THERMOPHORESIS IN PLATE HEAT EXCHANGER WITH HIGH SOLID CONTENT

U. Ojaniemi[1], M. Manninen[1], T. Pättikangas[1] and M. Riihimäki[2]

[1] VTT Technical Research Centre of Finland, P.O.Box 1000, FI-02044 VTT, FINLAND ulla.ojaniemi@vtt.fi
[2] Mass and Heat Transfer Process Laboratory, Department of Process and Environmental Engineering, University of Oulu, P.O. Box 4300, FI-90014 Oulu, FINLAND

ABSTRACT

Particulate fouling of plate heat exchangers is studied using a multiphase computational fluid dynamics (CFD) approach based on the algebraic slip mixture model. Particulate fouling is a serial process of transport of particles into a vicinity of the surface and then adherence on the surface. Turbulence is generally considered to be the main reason for resuspension of the adhered particles. The suitability of different turbulence models for describing the shear forces at wall when modelling fouling is investigated. CFD simulations of a test heat exchanger were performed with standard k-ε turbulence model with enhanced wall treatment (EWT) in 2D and 3D. Large Eddy Simulations (LES) in 3D were performed and compared to the k-ε model results. The calculated results were compared with the experimental data for deposition rate of colloidal calcium carbonate particles and with the results simulated with the CFD model for particulate fouling presented earlier by Ojaniemi *et al.* (2012). The earlier model incorporated the drag and diffusion forces affecting on the particle transport in the near-wall region into the wall function approach. Here, the model has been further developed to include the effect of thermophoresis. Several models presented in literature for the Soret coefficient are compared.

INTRODUCTION

The interest in modelling of fouling mechanisms has been increasing in the recent years, since fouling is associated with the increased costs of maintenance, downtime and oversizing of the process equipment (Kerner, 2011). In this paper, the particulate fouling of plate heat exchangers is studied. The particulate fouling process can be considered as a serial process of transportation into the vicinity of the wall, adherence on the surface and re-entrainment. The particle transport to the surface is calculated with a wall function approach based on convective-diffusion equation including the particle-wall interaction energy and the reduced mobility of the particle in the near-wall region presented earlier by Ojaniemi *et al.* (2012). The algebraic equation for solving the particle flux to the wall from the bulk volume fraction α_b far away from the wall was obtained

$$J_W = \rho_p K_f \left[1 - e^{J_W/B}\left(1-\alpha_b\right)\right] \quad (1)$$

where B is a parameter depending on the diffusion coefficients.

The adhesion of the particles on the wall is controlled by colloidal interaction forces. In the CFD model for the particulate fouling, the electrical interaction energy between the surfaces of the particles and the wall determines the amount of deposited mass on the wall. The methods of Spielman and Friedland (1973) and Elimelech (1995) were used for incorporating the interaction energy into the calculation of particle flux at the wall. The rate of adhesion is calculated in this method from the electrical interaction potential barrier with the pseudo-first-order rate constant

$$K_f = D_B \left\{ \int_0^{\delta_D} \left(g_1(H) e^{\phi_T / k_b T} - 1 \right) dy \right\}^{-1} \quad (2)$$

where $g_1(H)$ is the hydrodynamic correction factor and H is the normalized distance between the surfaces. The interaction potential $\phi_T = \phi_{vdw} + \phi_{edl} + \phi_{AB}$ is calculated as a total sum of the interaction potentials based on XDLVO (extended DLVO) theory. Adhesion is determined by the balance between the attractive and repulsive forces. The theory comprises the van der Waals potential, ϕ_{vdw}, and the interaction potential arising from electrical double layer, ϕ_{edl}, based on the DLVO theory of the colloid stability developed by Derjaguin and Landau (1941), and the non-DLVO force of the attractive hydrophobic interactions, ϕ_{AB}, according to the model of van Oss (2006).

The simplified wall function model includes drag and diffusion, but thermophoresis, lift forces, particle interaction and resuspension were neglected. Turbulence is generally considered as the main reason for resuspension of the adhered particles. For modelling resuspension, the dynamic models based on energy accumulation due the transfer of turbulent energy are recently often applied, e.g., the model of Vainshtein (1997). The realistic modelling of turbulence is then essential. Here, the CFD simulations of a test heat

exchanger were performed with LES in 3D and compared to the results calculated with standard *k-ε* model with EWT in 2D and 3D. The calculated results were compared with the experimental data for deposition rate of colloidal calcium carbonate particles presented by Ojaniemi *et al.* (2012).

In addition, the model has been further developed to include the effect of thermophoresis, which is the force due temperature gradient affecting the particle transport. Thermal diffusion of charged colloids is mainly caused by properties of the electrolyte solution (Würger, 2009). Thermophoresis of particles in liquids has been extensively studied during the recent years (Putnam, 2007; Würger, 2009), but a generally accepted theory for thermophoresis has not been established. Several models presented for the Soret coefficient in literature are compared.

TURBULENCE MODELLING WITH LES

Since the large scale turbulent eddies contain most of the energy and account for most of the turbulent transport, they dominate the main properties of the turbulent flow. The large scales are problem-dependent and difficult to model, whereas the smaller scales become more and more universal and can be modelled more precisely. In LES, the large eddies are resolved numerically, and only the small scale eddies having a slight effect on the large scale eddies are modelled with sub grid scale model (SGM). Thus, the success of the LES simulation is dependent on the performance of the sub grid model.

The wall-bounded flows, as in the case of heat transfer, are demanding situations for LES modelling. The turbulent length scales near the wall are dependent on the distance from the wall, i.e., near the wall the length scale of the largest eddies is small. Therefore, high resolution of the grid is needed near the wall. As the Reynolds number increases, the thickness of the viscous layer dampening the turbulence decreases, and the need for high resolution grid is increased. Thus, the wall-bounded flows modelled with LES are limited to flows of low Reynolds number, around Re ~10^4-10^5 (Fluent, 2011).The typical resolution requirements for LES are (Menter, 2011):

$$\Delta x^+=40,\ \Delta z^+=20,\ N_y=60\text{-}80 \qquad (3)$$

where Δx^+ is the non-dimensional grid spacing in the streamwise direction, Δz^+ in the spanwise and N_y the number of cells across half of the channel height. The definition for the non-dimensional grid spacing, e.g., for the streamwise direction is $\Delta x^+ = u_\tau \Delta x/\nu$, where u_τ is friction velocity and ν is kinematic viscosity of the fluid. In addition to the grid resolution, the needed CPU power increases with increasing Reynolds number, as the time step Δt also needs to be reduced to maintain a small Courant number, $CFL=U\,\Delta t/\Delta x$, where U is bulk fluid velocity.

The classical and widely applied Smagorinsky sub grid model is not applicable in wall bounded flows due to the excessive dampening of the large scale eddies near the wall without correcting the model parameters. The Wall-Adapting Local Eddy-Viscosity (WALE) model returns the correct near wall behaviour of turbulent viscosity ($\propto y^{+3}$) for wall bounded flows (Fluent, 2011). In addition, WALE returns a zero turbulent viscosity for laminar shear flows, in contrast to the Smagorinsky model. From the models provided by Fluent, the WALE model is then preferable model for the sub grid model of LES in the studied case.

WALL FUNCTION APPROACH WITH THERMOPHORETIC FORCE

The starting point for the wall function model for fouling is the assumption of the local equilibrium implying that the particles move always with their terminal velocity. This means that the particles are presumed to accelerate to the terminal velocity infinitely fast. The assumption is accurately valid for small colloidal particles in a liquid. The equation for the slip velocity is

$$0 = \mathbf{F}_{tot} + \left(\rho_p - \rho_q\right)\left[\mathbf{g} - \left(\mathbf{u}_m \cdot \nabla\right)\mathbf{u}_m\right] \qquad (4)$$

where *m* refers to mixture and F_{tot} is the total force affecting particle transport.

The dominating forces and mechanisms in transporting the colloidal particles are Brownian and turbulent diffusion, drag, lift and thermophoretic forces. The lift force was neglected as insignificant in comparison to the diffusion force (Ojaniemi *et al.*, 2008). Therefore, the total force affecting particles is composed

$$\mathbf{F}_{tot} = \mathbf{F}_{diff} + \mathbf{F}_{drag} + \mathbf{F}_{th} \qquad (5)$$

The forces are expressed by

$$\mathbf{F}_i = K_{pq}\mathbf{u}_i \qquad (6)$$

where K_{pq} is the interphase momentum exchange coefficient.

In the diffusion velocity calculated based on Fick's law, the Brownian and turbulent diffusivities, D_B and D_t have been included. The thermophoretic velocity is calculated by thermal diffusivity $D_{th}=S_{th}D_B$, where the Soret coefficient S_{th} is a model and temperature dependent coefficient.

In equation (4), the term due to velocity gradients can be neglected close to the wall. Only the direction perpendicular to the wall (the y-component) is of interest. The acceleration term is also small because the mixture velocity in the *y*-direction and the *x*-derivative of the mixture velocity are small. Only the perpendicular component of gravitation **g** to the wall is important, although in colloidal system insignificant. The equation for the *y*-component of the slip velocity is then

$$v_{slip} = -\left(\frac{D_B + D_t}{\sigma \alpha_p \alpha_q}\right)\frac{\partial \alpha_p}{\partial y} - S_{th}\frac{\partial T}{\partial y} + \frac{\left(\rho_p - \rho_q\right) g_y}{K_{pq}} \qquad (7)$$

where the Stokes expression is applied for the interphase momentum exchange coefficient, K_{pq}.

Close to the wall, the form of the continuity equation proposed by Johnsen and Johansen (2010) is applied:

$$\frac{\partial}{\partial y}\left(\alpha_p \rho_p v_p\right) = -\frac{J_W}{y_b}. \qquad (8)$$

where ρ_p is the particle density and y_b is a distance beyond the particle boundary layer. Integration from $d_p/2$ to *y* gives

$$-\alpha_p \rho_p v_p = J_W\left(1 - \frac{y}{y_b} + \frac{d_p}{2y_b}\right) \qquad (9)$$

In order to complete the model, temperature wall function is also needed. With the assumption that the

temperatures of fluid and particles are equal, the enthalpy equation is

$$\nabla\cdot\left(\alpha_p\rho_p\mathbf{u}_p h_p+(1-\alpha_p)\rho_q\mathbf{u}_q h_q\right)=\nabla\cdot\left(\lambda_{eff}\nabla T\right) \quad (10)$$

where λ_{eff} is the effective heat transfer coefficient and h_i is the sensible enthalpy of phase *i*. Next it is approximated that the liquid velocity perpendicular to the wall is small and can be neglected. The specific heat is assumed to be constant so that

$$h_p=h_{p,ref}+c_{pp}\left(T-T_{ref}\right) \quad (11)$$

Integrating Eq. (10) and denoting the wall heat flux by q_W (positive towards the wall), it follows

$$q_W=\lambda_{eff}\frac{\partial T}{\partial y}-\alpha_p\rho_p v_{slip}\left[c_p\left(T-T_W\right)\right] \quad (12)$$

The effective heat transfer coefficient is written as

$$\lambda_{eff}=\frac{c_{pm}\mu_t}{\mathrm{Pr}_t}+\alpha_p\lambda_p+\alpha_q\lambda_q \quad (13)$$

where the default value for Pr_t is 0.9. Combining equation (9) with equation (10) and with $v_p=v_{slip}$ from equation (7) gives

$$q_W=\lambda_{eff}\frac{\partial T}{\partial y}+J_W\left(1-\frac{y}{y_b}+\frac{d_p}{2y_b}\right)c_{p,p}\left(T-T_W\right) \quad (14)$$

Solving for $\partial T/\partial y$ and inserting in (9) with $v_p=v_{slip}$ from equation (7) results in

$$\rho_p\left(\frac{D_B+D_t}{\sigma\alpha_q}\right)\frac{\partial\alpha_p}{\partial y}+\alpha_p\rho_p S_{th}\frac{q_W}{\lambda_{eff}}-\alpha_p\rho_p\tau_p g_y=J_W\left(1-\frac{y}{y_b}+\frac{d_p}{2y_b}\right) \quad (15)$$

where $\tau_p=d_p^2(\rho_p-\rho_q)/(18\mu)$. The convective term in the heat transfer equation is considered to be negligible. The solution for the equation (15) is obtained by assuming the temperature dependent physical fluid properties to be constant at the wall temperature. This assumption is valid, because the wall function model operates in the near-wall region $y^+ < 3$, where the change in the temperature is of the order of few degrees. The turbulent kinematic viscosity profile near the wall is obtained from Johansen (1991).

The final algebraic equation for solving the particle flux to the wall from the bulk volume fraction α_b far away from the wall is

$$J_W=\rho_p K_f\left[\frac{Z-J_W e^{J_W/B}\left(1-\alpha_b\right)}{Z+(c-s)e^{J_W/B}\left(1-\alpha_b\right)}\right] \quad (16)$$

where $Z=J_W+(c-s)\alpha_b$, $c=\rho_p v_{sg}$, $s=\rho_p S_{th}q_W/\lambda_{eff}$ and *B* is a parameter depending on the diffusion coefficients (Ojaniemi *et al.*, 2012).

MODELS FOR THERMOPHORETIC COEFFICIENT

For calculating the Soret coefficient of the thermophoretic force in a liquid, several models are available in the literature, but the proposed models give markedly different results. Some of the presented models for Soret coeficient are tested here. Fig. 1 shows the Soret coefficients as a function of temperature predicted by several models from literature: Parola and Piazza (2004), Putnam *et al.* (2007), Dhont *et al.* (2007), Würger (2009) and Semenov *et al.* (2011).

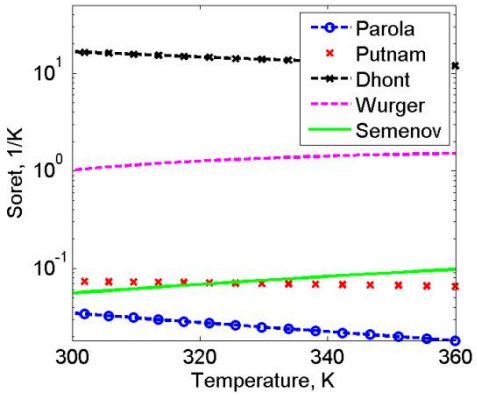

Fig. 1. Soret coefficients predicted with several models, 1/K.

Fig. 1 shows the wide range of the models for the Soret coefficients. The models are for charged colloids in liquid, most often based on a single particle theory, and the particle-particle interactions are not included. It has also been found that the thermal diffusion can have different signs in different circumstances. The sign of the coefficient in the model of Semenov *et al.* (2011) was explained by the dominating contribution of electrostatic interaction in a double layer or Hamaker interactions of the suspended colloid particle. Würger (2009) proposed the temperature dependence of the sign of Soret coefficient to arise from thermoelectric contribution. Several studies of the nanoparticle suspensions have shown similar particle behaviour: particles are moving towards the hot wall when the bulk temperature is low, e.g. below 293K (negative coefficient) and towards the cold side if the bulk temperature is more than 303 K (Putnam, 2007, Würger, 2009).

Several models were chosen for further study with particulate CFD fouling model in order to evaluate the magnitude of the thermophoresis in comparison to other forces affecting particle transport. The results are shown for the models Parola and Piazza (2004), Putnam *et al.* (2007) and Würger (2009). The modelled coefficients are taken positive due to the bulk temperature 333 K applied in the experiments, i.e. thermophoresis has been considered as a cleaning mechanism.

Parola and Piazza (2004) have proposed for charged colloids the following form of the Soret coefficient for coupling the heat and mass transfer in liquids

$$S_{T\_PP}=\frac{\varepsilon d_p}{2k_b T^2}\zeta_p^2, \quad (17)$$

where ζ_p is the electrical surface potential of the spherical $CaCO_3$ particle and ε is the permittivity of water.

In the model of Putnam *et al.* (2007), the model of Anderson is approximated with the electric field of a flat double layer. The model of Anderson is based on the

Derjaguin model of the thermo-osmosis of an electrolyte in a porous medium. Anderson then derived the model to describe the thermophoresis of particles in liquids. In the modified model of Putnam *et al.* (2007), the electrostatic field due to the polarization of water molecules in the double layer is included into the model resulting in

$$S_{T\_P} = \frac{3\pi d_p}{4k_b T^2}\left(1+\frac{\lambda_p}{2\lambda_q}\right)^{-1}\left(\varepsilon + T\frac{\partial\varepsilon}{\partial T}\right)\zeta_p^2 \qquad (18)$$

with the restrictions $\zeta \le 2k_bT/e$ and $\kappa d_p/2 >> 1$.

Würger (2009) has proposed that for charged colloids in aqueous solutions the electric forces dominate in comparison to dispersion forces. The model for Soret coefficient is thus

$$S_{T\_W} = \frac{\varepsilon\zeta_p}{\mu_q T}\left(\frac{\zeta_p}{3} - \delta\alpha\frac{k_bT}{e}\right)D_B^{-1} \qquad (19)$$

where $\delta\alpha(T) = 0.8 + 0.025K^{-1}(T - 298K)$. The first term accounts for the flow of the electric energy density in a temperature gradient, and the second term results from the thermoelectric field.

EXPERIMENTAL ARRANGEMENT

The results from the fouling test apparatus described by Riihimäki *et al.* (2010) were used for the validation of the particulate fouling model. The test section consists of a rectangular flow channel, which has a flow area of 15 × 100 mm^2 and a length of 0.95 m (see Fig. 2). Two removable test plates of area 100 × 200 mm^2 are mounted in the test section. The test plates are placed on a 25 mm thick copper block with embedded ohmic heaters. From the agitated vessel of 150 dm^3, particle suspension is pumped to the test section through a double pipe heat exchanger, which controls the temperature of the test fluid.

By keeping the heat flux and wall temperature constant, deposition of the resistive layer on the wall can be measured from the increase of temperature in the joint between the heating block and the test plate. In the experiments, the dispersed suspension of grounded lime stone diluted with de-ionized water to the desired concentrations was applied as test fluid. A more detailed presentation of the experimental arrangements is found in Riihimäki *et al.* (2010).

For testing the particulate fouling model, the experiment with mass flow rate 0.5 lps, particle concentration 5.5 vol% (s.c. 13.9 wt%) and heating rate 21 kW/m^2 was chosen (Ojaniemi *et al.*, 2012). The averaged time period for experimental test was 3.5 h. Temperature of the mixture was 333 K at the inlet of test section. The viscosity of the mixture was taken as two times the water viscosity, with the same temperature dependence as water viscosity. The material properties applied are presented in Table 1. For particle size, a representative diameter was chosen (see Ojaniemi *et al.*, 2012). The surface is assumed to be fouled, and the deposition rate on the fouled surface is simulated.

The algebraic slip mixture model of Fluent 14.0 was applied for the time dependent multiphase simulation (Fluent, 2011). The particle-particle interaction was included by applying the granular particle model based on kinetic theory. The model takes into account the maximum packing density of particles in the fluid. Temperature dependent models were used for the water density (Perry, 1970) and water viscosity (Kell, 1975). The Reynolds number of the simulated case was 6200.

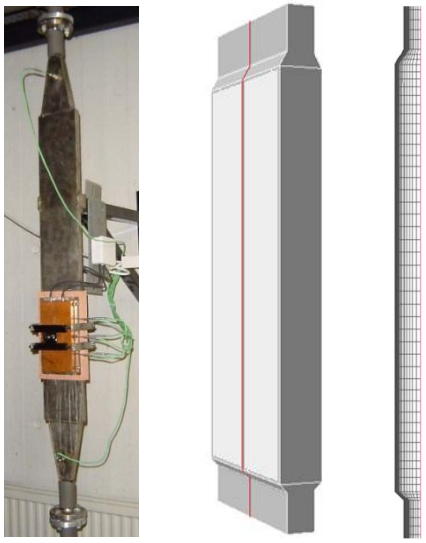

Fig. 2. Test apparatus, geometry in 3D and 2D grid applied in simulations. Red line illustrates the placement of the 2D grid in the geometry. The light, flat wall shown in the middle picture is the heated surface.

Table 1. Material parameters

Density of particles ($CaCO_3$)	2711 kg/m^3
Zeta potential of particles	–18 mV
Thermal cond. of particles	2.7 W/(mK)
Thermal cond. of water	0.6 W/(mK)
Ion strength	0.044 mol/dm^3
Slurry viscosity	2 × water visc., kg/(ms)
Representative diameter of particles	387 nm

COMPARISON OF 3D SIMULATION RESULTS WITH LES AND *k-ε* RANS MODEL

The three-dimensional computational grid used consisted of 1.2 million cells. The non-dimensional grid spacings at the wall were $\Delta x^+ \sim 40$, $\Delta z^+ \sim 10$ and $\Delta y^+ \sim 0.7$. With time step 0.0075 s, the Courant number was around 0.4 in the near wall region. The simulations were carried out with LES model applying the WALE model for sub grid turbulent viscosity. For the momentum conservation, the bounded central discretization method was applied, for volume fraction the second order discretization and for time discretization, the implicit second order method was used.

In the simulations, the inlet profiles for turbulent kinetic energy and dissipation, and velocity were calculated separately with CFD applying the standard *k-ε* with EWT for turbulence modelling. The inlet boundary condition of introducing vortex instabilities into the flow was applied in LES simulation for producing the turbulent flow. Fig. 3

shows, how the unsteady turbulent flow develops into the domain. In Fig. 4, the sub grid turbulent viscosity is presented at the heated wall. The turbulent viscosity resulting from the modelling of the small scales eddies is insignificant implying that the relevant turbulence is resolved in the grid. A smaller eddy viscosity to viscosity ratio is predicted with LES than with the *k-ε* model with EWT, showing the LES modelling to be appropriate.

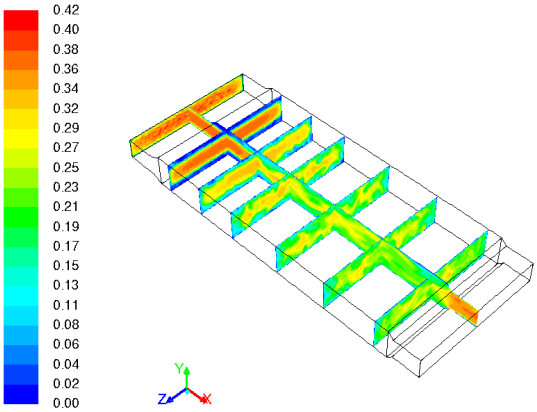

Fig. 3. Instantaneous velocity magnitude, m/s, LES. Flow is in the direction of x-axis.

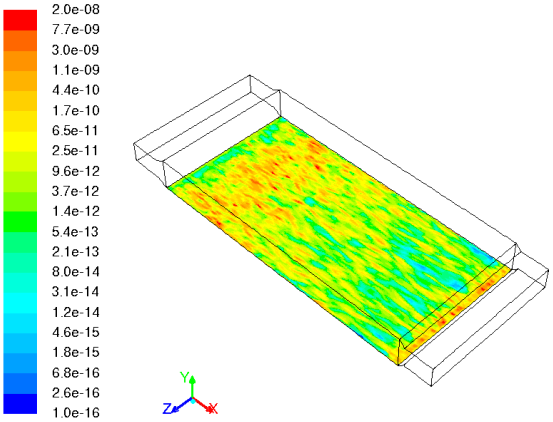

Fig. 4. Profile for instantaneous sub grid turbulent viscosity at the heated wall. Logarithmic scale.

For comparison of the results with LES, the standard *k-ε*-model with EWT was used for modelling turbulence in the same case with same grid and time step. For the momentum conservation, the second order discretization was applied. For realistic modelling of the inlet flow field, the profiles for inlet velocity, particle distribution, turbulent kinetic energy and dissipation calculated separately for LES were applied.

In Fig. 5 and 6, the results for velocity magnitude in the heat exchanger are shown for simulation with LES and with standard *k-ε* model with EWT. The results for LES are time averaged from the simulation period of 72.4 s. The profiles for the results are quite different. LES model predicts the high-velocity flow to penetrate a longer distance into the domain than *k-ε* model. This is also seen in the shear stress at the heated wall, Fig. 7.

Fig. 8 compares the temperature distributions at the heated wall. Since the flow velocity profiles are different, the resulting temperature distributions also differ. The temperature increases near the edge of the inlet as the flow is less mixed.

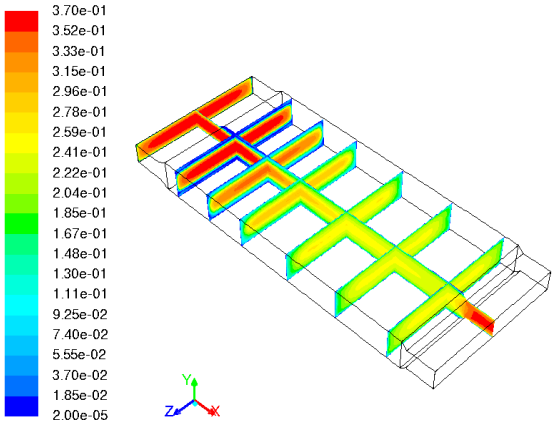

Fig. 5. Velocity magnitude, m/s. LES, time averaged result. Flow is in the direction of *x*-axis.

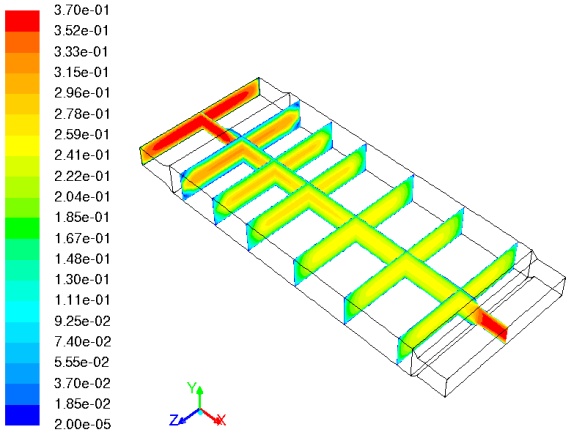

Fig. 6. Instantaneous velocity magnitude, m/s. Standard *k-ε* with EWT. Flow is in the direction of *x*-axis.

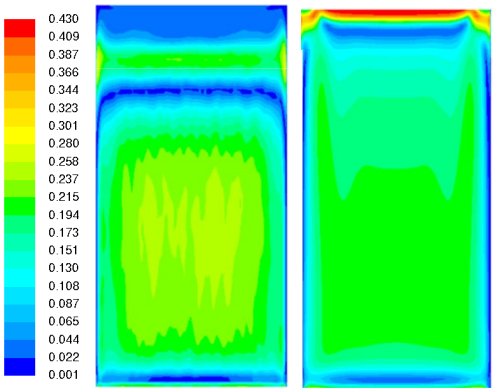

Fig. 7. Shear stress at the heated wall, Pa. On the left: LES, time averaged result. On the right: standard *k-ε* with EWT. Flow is directed downwards.

The different results produced by the models are also seen in the distribution of deposits at the heated wall, see Fig. 9. The LES model predicts stronger fouling rate at the edge of the heated wall near the inlet. According to the results with standard *k-ε*-model with EWT, the fouling rate is higher in the corners near the outflow.

Examples of the deposition on test plates in experiments are shown in Fig. 10. The experiments were

done with higher particulate concentration of 50.7 % where the non-uniform deposition is clearly seen. Qualitatively the deposition profiles are closer to the results of the LES simulation showing the region with decreased fouling rate to be further away from the flow inlet.

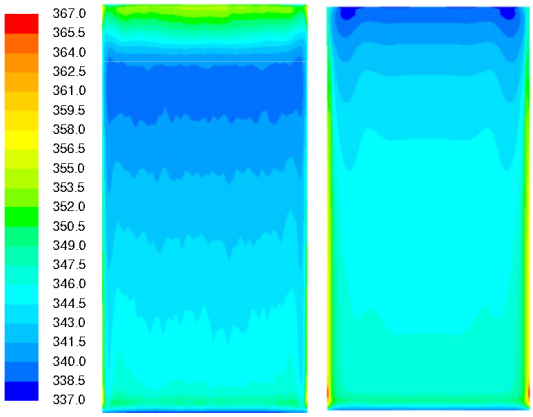

Fig. 8. Temperature at the heated wall, K. On the left: LES, time averaged result. On the right: standard k-ε with EWT. Flow is directed downwards.

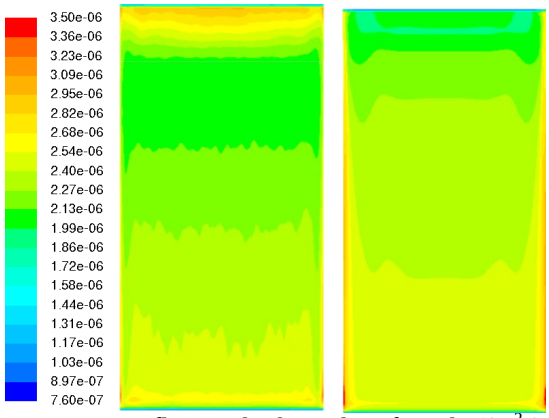

Fig. 9. Deposition flux to the heated surface, kg/(m^{2}s). On the left: LES, time averaged result. On the right: standard k-ε with EWT. Flow is directed downwards.

Fig. 10. Experimental results for deposition profiles. On the left: T_{fluid}=353 K, 0.8 lps, 20 kW/m^2, s.c. 50.7%. On the right: T_{fluid}=333 K, 0.45 lps, 30.2 kW/m^2, s.c. 50.7%. Flow is directed downwards.

2D SIMULATION RESULTS WITH THERMOPHORESIS

The applied two-dimensional asymmetric computational grid consisted of 1120 cells. With the wall cell size of 0.15 mm, the y^+ value of about 1 was obtained. The standard k-ε-model with EWT was used for turbulence. The profiles for inlet velocity, particle distribution, turbulent kinetic energy and dissipation were calculated in a separate CFD calculation.

The wall function approach including thermophoresis was implemented in Fluent 14 with user defined functions (UDF). In order to evaluate the need to include the thermophoresis also into the outer region of the near wall, comparison of the forces due to turbulent diffusion and thermophoresis was carried out. The results are shown in terms of the corresponding accelerations a_{th} and a_{tdiff} derived from the calculated forces per unit volume, e.g. for acceleration due to thermal forces

$$a_{th} = \frac{\mathbf{F}_{th}}{\alpha_p \rho_p} \qquad (20)$$

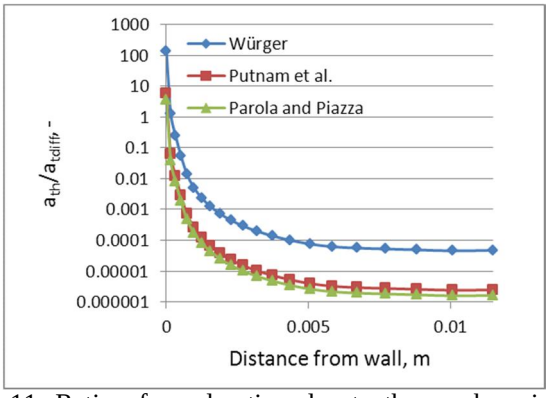

Fig. 11. Ratio of acceleration due to thermophoresis, a_{th}, and acceleration due to turbulent diffusion, a_{tdiff}, as a function of distance from the heated wall. Results are calculated using three different Soret coefficient models.

Fig. 11 shows the relative acceleration due thermophoresis in comparison to acceleration due to turbulent diffusion for the three Soret coefficients. According to models of Parola and Piazza (2004) and Putnam *et al.* (2007), the effect of thermophoresis in comparison to turbulent diffusion is restricted only into the cells adjacent to wall. With the model of Würger (2009), the effect penetrates deeper into the domain. However, we included the thermophoresis only into the near wall region in the wall function approach.

In Fig. 12, the deposition rate calculated including the thermophoresis on the heated wall is shown as a function of distance from inlet. For comparison, the simulation results without the thermophoresis for the same case are shown. The models of Putnam *et al.* (2007) and Parola and Piazza (2004) seem to have only minor effect on the deposition rate in the simulated case. The model of Würger (2009) predicted greater effect, and the effect would be even greater if thermophoresis would be included in the domain next to the cells adjacent to the heated wall. In comparison to the experimental values (Ojaniemi *et al.* 2012), the effect of Würger model seems to be too strong. For comparison,

the results taken from the middle of the plate of 3D simulations are also included in Fig. 12 (see Fig. 2).

In Fig. 13, the differences of the predicted deposition rates with the applied models in comparison to the results with standard *k-ε* with EWT in 2D are presented. The values are presented also in Table 2. The averaged experimental value was 130 mg/m^2/min.

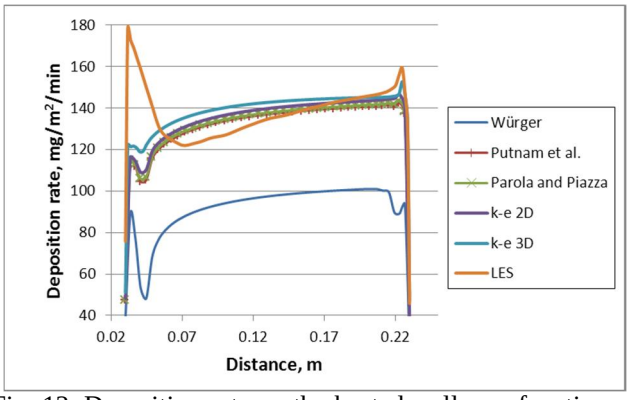

Fig. 12. Deposition rate on the heated wall as a function of distance from inlet, mg/m^2/min.

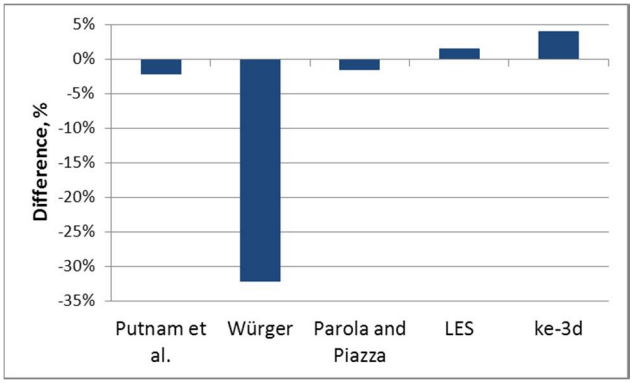

Fig. 13. Differences of the predicted deposition rates with the applied models in comparison to the results with standard *k-ε* with EWT model in 2D.

Table 2. Deposition rates predicted with the applied models

	mg/m^2/min	%
k-ε, 2D, no Soret	136	
Putnam *et al.*	133	-2.2
Würger	92	-32.1
Parola and Piazza	134	-1.5
k-ε , 3D	141	3.9
LES, 3D	138	1.4
Experiment	130	

DISCUSSION

The simulation results in 3D with LES and standard *k-ε* turbulence model with EWT for temperature and velocity magnitude profiles were quite different affecting the deposition rate profile at the heated wall. The increased deposition rate in the corners of the heat exchanger resulted in increased fouling rate with the standard *k-ε* EWT model in 3D.

The applied models for thermophoresis seem to have only little effect on deposition rate, except the model of Würger (2007). In comparison to the experimental results, the predicted deposition rate with the model of Würger (2007) was only 71%, and 68% in comparison to the simulation results without thermophoresis. The difference of the results with Parola and Piazza (2004) or Putnam *et al.* (2007) in comparison to the experimental values was only of the order of 1%.

The deposition rate due to crystallization is not included in the model. However, with the applied test fluid, the supersaturation ratio of $CaCO_3$ is low and therefore, the significance of the crystallization would be probably low, as discussed in Ojaniemi *et al.* (2012). In order to produce measurable crystallization fouling rate in the experiments in comparable conditions, the $CaCO_3$ concentration has been an order of magnitude greater (Pääkkönen *et al.*, 2010). The effect of ions on the fouling rate is taken into account in the parameters of XDLVO theory: the zeta-potential of particles and the ion strength.

Including the particle size distribution in the simulation would be computationally demanding. Therefore only the estimated effective particle size was applied. The particle size distribution has known to have an effect on the deposition rate: smaller particles reinforce the fouling.

The resuspension of the particle occurs, when the energy of particle is sufficient to exceed the energy due to the adhesive potential well. The particle resuspension model proposed by Vainshtein (1997) is based on the particle reentrainment by a turbulent fluid drag force. Here the surface was assumed to be smooth. The re-entrainment of the particles is not taking place according to the model of Vainshtein (1997) with the shear stress levels found at the heated wall, see Fig. 7. If the surface roughness is included, the resuspension of the particles might take place, and the resulting deposition rate would be lower.

CONCLUSIONS

The effect of the turbulence on the particulate deposition was studied by comparison of the results with LES and standard *k-ε* with EWT in 3D simulation in a case of the plate heat exchanger with a moderately high concentration of suspended calcite particles. The resulting profiles for the deposition distribution were markedly different. In comparison to the deposition distribution on test plates in experiment with high solid contents, the result of the LES simulation seems to be more realistic.

The wall function approach for particulate fouling for CFD modelling was further developed to account also the force due to thermophoresis. The model comprising of diffusion and drag has been presented earlier in Ojaniemi *et al.* (2012). As a conclusion, the model incorporates now the most important forces having effect on the colloidal particles transport near the heated wall. The model is applicable to practical industrial heat exchangers based on parameters taken from literature or experiments. In further studies, the wall roughness, and the effect of crystallization should be incorporated into the model.

NOMENCLATURE

a acceleration, m/s^2
c thermal conductivity, W/(m K)
d_p particle diameter, m
D diffusion coefficient, m^2/s
F force, N/m^3
h sensible enthalpy,
J_W flux, kg/(m^{2}s)
k_b Boltzmann constant, $1.3807 \cdot 10^{-23}$ J/K
K_f mass transfer rate, m/s
K_{pq} interphase momentum exchange co., kg/(m^{3}s)
q_W heat flux, W/m^2
T temperature, K
u velocity, m/s
v velocity, m/s
y distance from surface, m
α volume fraction, dimensionless
ε permittivity, C^2/(m J)
ζ electrical surface potential, V
λ thermal conductivity, W/(m K)
μ viscosity, kg/(m s)
σ Prandtl constant, 0.9
ρ density, kg/m^3
ϕ interaction energy between surfaces, J

Subscript

b bulk
eff effective
p particle
q liquid
t turbulent
y directed in y coordinate

ACKNOWLEDGEMENT

The MATERA+ ERA-Net co-operation by the Functional materials programme of Tekes, the INTER programme of FNR, and industrial partners e.g. Andritz, Oerlikon Balzers and Outokumpu are acknowledged for financially supporting the project.

REFERENCES

Derjaguin, B.V., Landau, L.D., 1941, *Acta Physicochim* Vol. 14, pp. 733.

Dhont, J. K. G., Wiegand, S., Duhr, S., Braun, D., 2007, Thermodiffusion of charged colloids: Single-particle diffusion, *Langmuir* Vol. 23, pp. 1674-1683.

Elimelech, M., Greory, J., Jia, X., Williams, R.A., 1995, Particle Deposition and Aggregation - Measurement, Modelling and Simulation, Elsevier.

Fluent, 2011, Ansys Fluent Users' guide – Release 14.0. Ansys Inc.

Johansen, S.T., 1991, The deposition of particles on vertical walls, *Int. J. Multiphase Flow* Vol. 17, pp. 355-376.

Johnsen, S.G., Johansen , S.T., 2010, Deposition modeling from multi-phase dispersed flow – A boundary layer wall function approach, *Proceedings of 8th International Conference on Heat Exchanger Fouling and Cleaning VIII – 2009 (Peer-reviewed)*, eds. H. Müller-Steinhagen, M. R. Malayeri, and A. P. Watkinson, EUROTHERM Seminar No. 86, 2009, pp. 237–244.

Kell, G.S., 1975, Density, thermal expansivity, and compressibility of liquid water from 0˚ to 150˚C: Correlations and tables for atmospheric pressure and saturation reviewed and expressed on 1968 temperature scale, *J. Chem. Eng. Data* Vol. 20, pp. 97-105.

Kerner, J., 2011, Compact, high-efficiency heat exchangers: Understanding fouling, *Chem. Eng*. Vol. 118, pp. 35-41.

Menter, F.R., 2011, Best Practice: Scale-Resolving Simulations in ANSYS CFD, ANSYS Germany GmbH

Ojaniemi, U., Pättikangas, T., Riihimäki, M., Manninen, M., 2008. CFD model for particulate fouling – modelling particle adhesion on surface with XDLVO theory, in: S.T. Johansen (Ed.), 6th Int. Conf. on CFD in Oil & Gas, Metallurgical and Process Industries, SINTEF/NTNU, Trondheim, Norway.

Ojaniemi, U., Riihimäki, M., Manninen, M., Pättikangas, T., 2012, Wall function model for particulate fouling applying XDLVO theory, *Chem. Eng. Sci.* Vol. 84, pp.57-69.

Parola, A., Piazza, R., 2004, Particle thermophoresis in liquids, *Eur. Phys. J. E* Vol. 15, pp.255-263.

Perry, J.H., 1970, Chemical Engineer´s Handbook, McGraw-Hill, New York.

Putnam, S.A., Cahill, D.G., Wong, G.C.L., 2007, Temperature dependence of thermodiffusion in aqueous suspensions of charged nanoparticles, *Langmuir* Vol. 23, pp. 9221-9228.

Pääkkönen, T.M., Riihimäki, M., Puhakka, E., Muurinen, E., Simonson, C.J., Keiski, R.L., 2010, Crystallization fouling of $CaCO_3$ – Effect of bulk precipitation on mass deposition on the heat transfer surface, *Proceedings of 8th International Conference on Heat Exchanger Fouling and Cleaning VIII – 2009 (Peer-reviewed)*, eds. H. Müller-Steinhagen, M. R. Malayeri, and A. P. Watkinson, EUROTHERM Seminar No. 86, 2009, pp. 209–216.

Riihimäki, M., Ojaniemi, U., Pättikangas, T.J.H., Pääkkönen, T.M., Manninen, M., Puhakka, E., Muurinen, E., Simonson, C.J., Keiski, R.L.,2010, Fouling in high solid content suspension – Effect of nucleating air and background electrolyte, *Proceedings of 8th International Conference on Heat Exchanger Fouling and Cleaning VIII – 2009 (Peer-reviewed)*, eds. H. Müller-Steinhagen, M. R. Malayeri, and A. P. Watkinson, EUROTHERM Seminar No. 86, 2009, pp. 192–199.

Semenov, S. N., Schimpf, M. E., 2011, Thermodynamics of mass transport in diluted suspensions of charged particles in non-isothermal liquid electrolytes, *C.R.Mecanique* Vol 339, pp. 280-286.

Spielman, L.A., Friedlander, S.K., 1973, Role of electrical double layer in particle deposition by convective diffusion, *J. Colloid Interface Sci*. Vol. 46, pp. 22-31.

Vainshtein, P., Ziskind, G., Fichman, M., Gutfinger, C., 1997, Kinetic Model of Particle Resuspension By Drag Force, *Phys. Rew. Lett.*, Vol. 78, pp. 551-554.

Van Oss, C.J., 2006. Interfacial forces in Aqueous media, 2nd ed., Marcel Dekker, New York.

Würger, A., 2009, Temperature dependence of the Soret motion in colloids, *Langmuir* Vol. 25, pp. 6696-6701.